LAWRENCE
LIVERMORE
NATIONAL
LABORATORY

LLNL-TR-704981

ARES Modeling of High-foot Implosions (NNSA Milestone #5466)

O. A. Hurricane

October 11, 2016

Disclaimer

This work performed under the auspices of the U.S. Department of Energy by Lawrence Livermore National Laboratory under Contract DE-AC52-07NA27344.

Introduction

The documentation provided in this memo completes NNSA Milestone #5466

"Apply ASC codes to modeling ICF data from NIF" with completion criteria of "Complete when predicted integrated fusion performance (Y, DSR, Tion as a function of implosion speed), using the ARES ASC code with calibrated multi-frequency radiation drives is compared to a subset of High-foot DT implosion data."

Method

The ASC code ARES was applied to a subset of the High-foot DT implosion series [e.g. T.R. Dittrich, et al., *Phys. Rev. Lett.*, **112**, 055002, (2014); O.A. Hurricane, et al., *Phys. Plasmas*, **21**, 056314, 2014] in 1D and some select high mode (mode 100) 2D problems were also run. These simulations include the capsule only. The x-ray drive is provided by frequency dependent sources ("FDS") that come from post-shot integrated hohlraum-capsule simulations using HYDRA after a series of source conversion steps that "calibrate" the sources to experiments that determine the shock timing, shock speeds, and bang-time. The ARES models are based on the set of input deck tools referred to as the capsule assessment test suite (CATS) created by J. Hayes. When run with diffusion radiation transport, the simulations use the technique documented in LLNL Report COPD-2012-0705. A 60-group multi-frequency structure is used in both the 1D and 2D problems.

The 2D simulations run are done including capsule and DT ice layer surface roughness and low-mode shape. Drive asymmetry from the hohlraum was not included, so the choice was made not to model some of the implosions that exhibited highly asymmetric shape. In the case of the fastest thinnest shell high-foot implosion, shot N140819, the self-generated magnetic-field package was exercised in order to assess whether magnetic fields made any difference.

The series of shots on NIF chosen for this milestone are: N130501, N130812, N130927, N131119, N131219, N140120, N140520, N140707, and N140819. These high-foot implosions range in implosion velocity from 300 – 390 km/s and range over ablator thickness from 195 microns to 165 microns. In each simulation, the actual as-shot geometry and DT ice layer characterization was used. The data that these simulations are compared against is documented in H.-S. Park, et al., *Phys. Rev. Lett.*, **112**, 055001 (2014); O.A. Hurricane, et al., *Nature*, **506**, 343-348 (2014); T. Ma, et al., *Phys. Rev. Lett.*, **114**, 145004 (2015); and T. Doeppner, et al., *Phys. Rev. Lett.*, **115**, 055001 (2015).

1D Results

As expected, at low implosion speeds the simulations match the data fairly well, matching the simulated 1D yield at ~50% (i.e. YOC(1D) = 51.7%) as well as other measured quantities. As the implosion speed is increased the simulation predicts higher fusion performance that was actually measured. The tables and plots below summarize the data vs. simulation comparison (blue = ARES simulation & red = experiment).

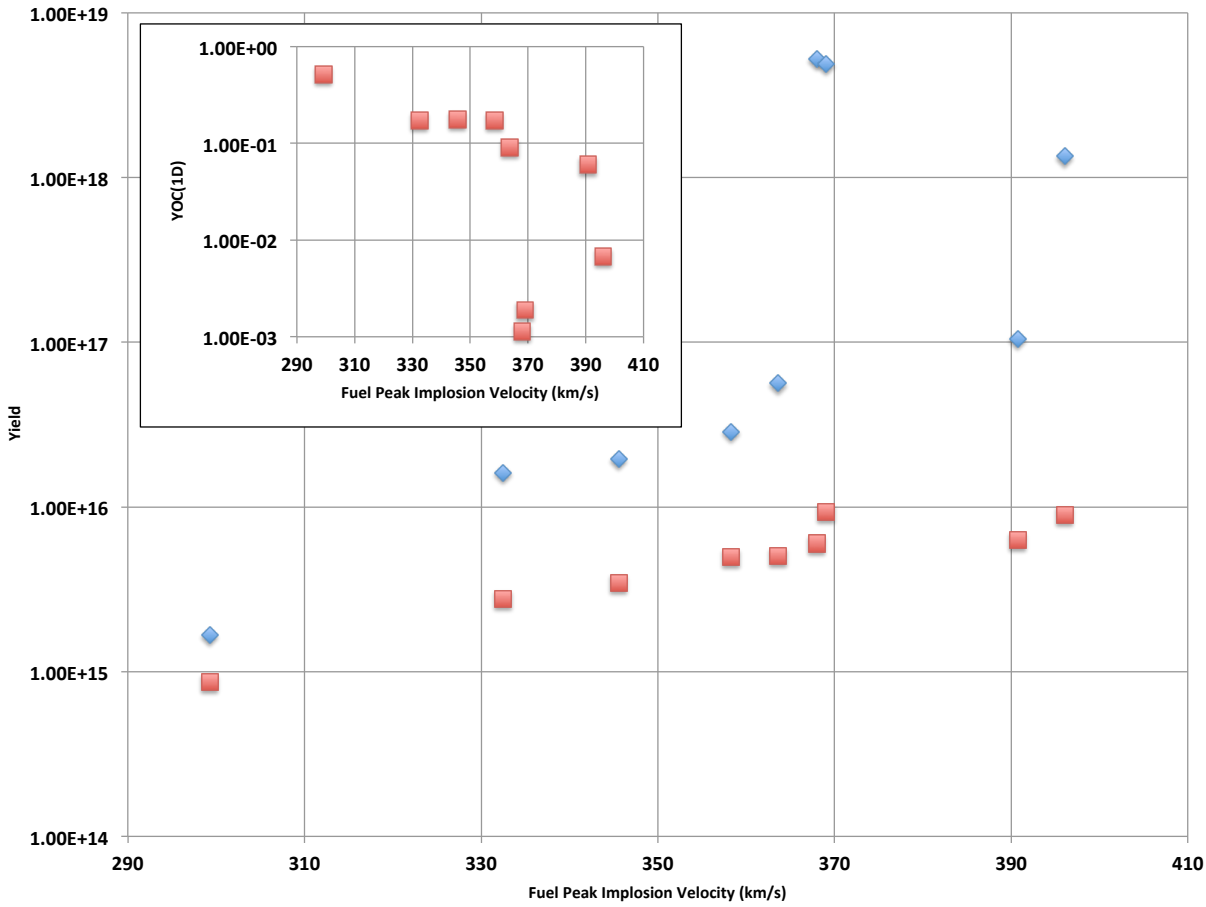

Figure 1: Total DT yield vs. fuel peak implosion velocity (as determined from the ARES 1D simulation). Above ~ 370 km/s second, the 1D simulation expects ignition/propagation level yields, while the data maxes out just below 1e+16 yields. Inset: Yield-over-clean (1D) is plotted against fuel peak implosion velocity and it shows the expected decline as the implosion speeds are increased. The igniting models stand out with especially low YOC(1D) < 0.01, while non-igniting models are in the 0.1-0.5 range of YOC(1D).

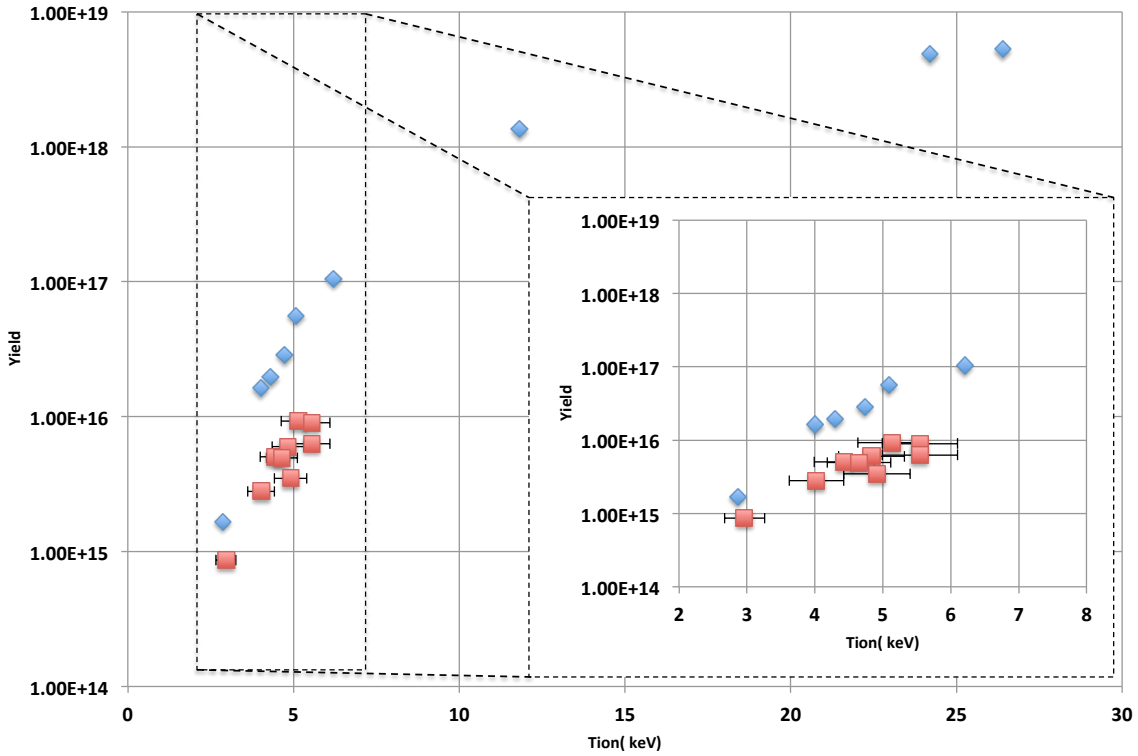

Figure 2: Total DT neutron yield is plotted against ion temperature. The igniting simulations show very high (>10 keV) ion temperatures. Without alpha-particle self-heating, ion temperature is essentially a reflection of implosion speed. Inset: A close-up view of the 2-8 keV region.

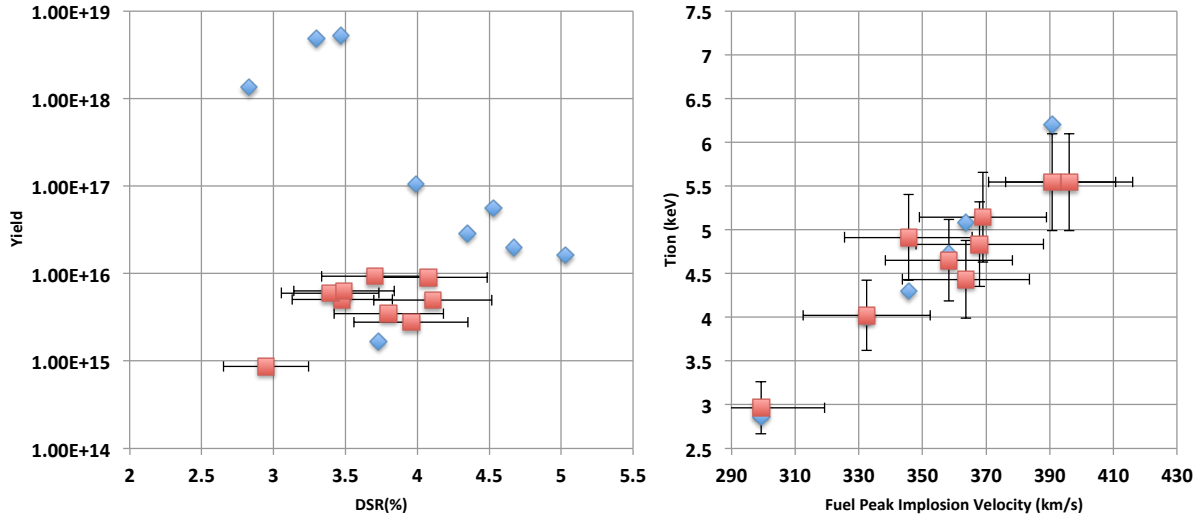

Figure 3: (Left) Total neutron yield vs. down-scatter ratio. Simulated yields and DSR's are generally larger than measured. (Right) Ion temperature vs. implosion speed. The agreement here is somewhat fortuitous since the simulated ion temperature is the neutron weighted average temperature, whereas the ion temperature from data is based upon the width of the neutron spectrum.

2D Results

Simulations of shots N131219 and N140819 are shown here as representative mid-velocity and high-velocity implosions with reasonably good symmetry. Since low-mode flux asymmetry is not included in these ARES simulations, it did not seem useful to model some of the more asymmetric implosions without including drive asymmetry. The impact of low-mode hohlraum drive asymmetry was assessed with HYDRA and documented (A.L. Kritcher, *et al.*, *Phys. Plasmas*, **23**, 052709, 2016) and it was determined that the primary degradation mechanism for these implosions was in fact the drive asymmetry.

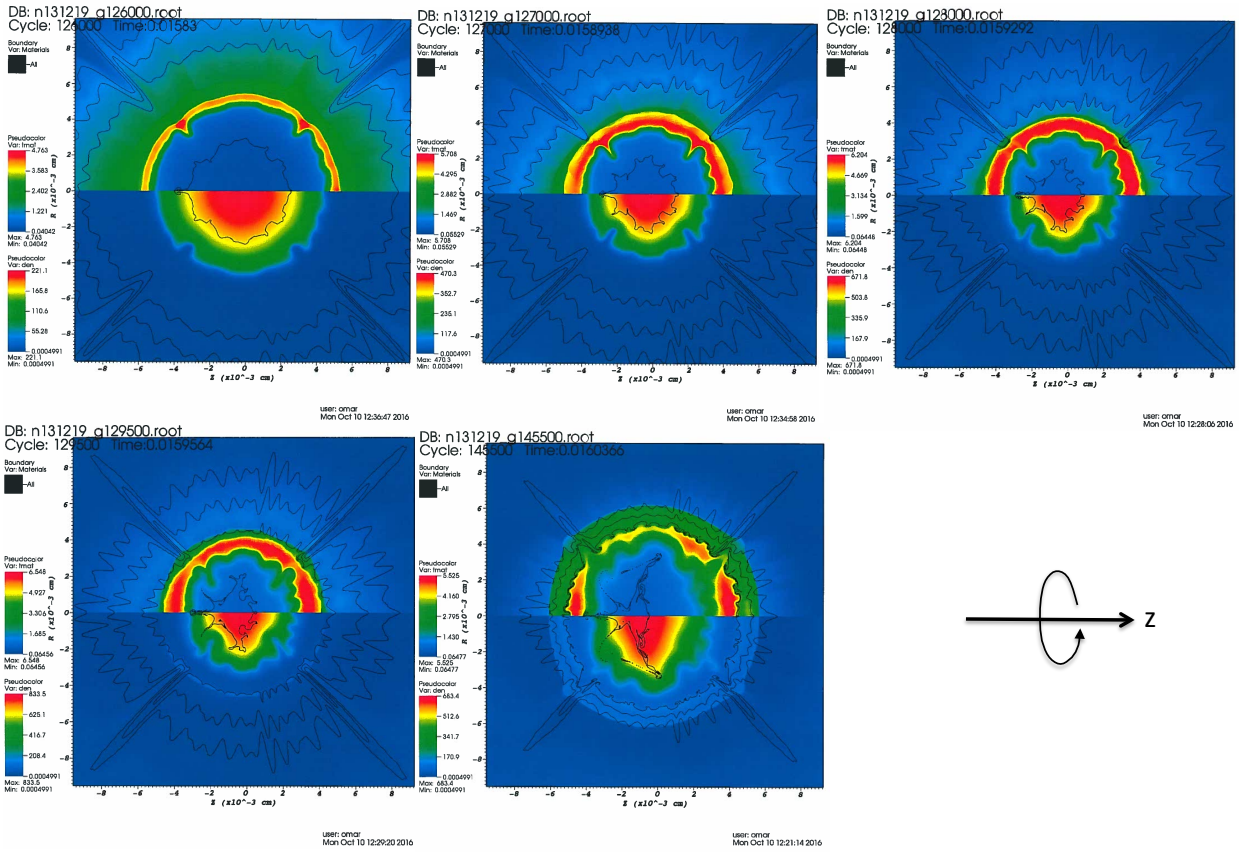

Figure 4: Images from 2D simulations of N131219 around bang-time. The upper half of each frame shows density (g/cc) and the lower half of each from shows ion temperature (keV). The impact on the morphology of the implosion of the tent perturbation is clearly visible – asymmetry in the shell and hot-spot amplify as the implosion compresses then disassembles. Black contours denote the boundaries between materials as defined at t=0, which from inside-out are the DT gas-ice interface, the DT ice – CH layer 1 interface, CH layer 2-3 interface, CH 3-4 interface, CH 4-5 interface, and CH layer 5 – He gas interface.

As a result of the tent being such a thin membrane of material (10's of nm), 15 nm specifically in the case of N131219, it cannot be resolved directly in a simulation with 1441 angular zones and

737 radial zones (1062071 total zones). So, the seed for the perturbation caused by the tent is mocked up using a surrogate perturbation that is calibrated to a one-time extremely high-resolution "direct" simulation performed by B. Hammel in HYDRA. The functional form of the surrogate perturbation is: $\delta r = -0.012319 \times 10^{-6}[\cos(2\phi)-0.04](\pi/2-\phi)^2\phi^2(\pi-\phi)^2/[1+0.99\cos(4\phi)]$. The fill-tube was not modeled here with ARES, but it has been examined previously [e.g. T.R. Dittrich, et al., *J. of Phys. Conf. Ser.*, **717**, 012013, 2016].

Some results of the N131219 tent simulation are shown in Figure 4 around the time of peak stagnation. The net simulated fusion metrics for N131219 with the tent are: Y = 2.45e16, T_{ion} = 4.6 keV, DSR = 3.4%, and BT (bang-time) = 15.98 ns – results which are not significantly different from the 1D model except for the DSR value (1D results: Y = 1.96e16, T_{ion} = 4.7 keV, DSR = 4.7%, and BT = 15.94 ns) which implies that the 2D effects of surface roughness and the tent, as modeled, are minimal. The DSR difference needs to be investigated, but could be the result of different radial resolutions between the 2D and 1D simulations or the 2D structure evident in Figure 4.

The effect of self-generated magnetic fields on N140819 was explored because N140819 was one of the fastest high-foot implosions and because the capsule included a symmetry breaking feature (a defect) in the ablator that leads to a the development of a large hydrodynamic finger-like structure that could create conditions favorable for magnetic field development. Arguably, this shot is the "best-case" for seeing magnetic field development.

Before running a simulation with magnetic fields a simple estimate was made in order to cross-check the ARES results. The Biermann Battery self-generated magnetic field equation is $\frac{d\boldsymbol{\Omega}}{dt} = \nabla P \times \frac{\nabla \rho}{\rho^2}$, where $\boldsymbol{\Omega}$ is the ion cyclotron frequency vector. Using a characteristic high velocity/high convergence high-foot implosion, typical values of scale-length are $L \sim 10^{-3}$ cm, $P \sim 10^{11}$ bar = 10^{17} dyne/cm^2, $\rho_{hot\text{-}spot}$ = 50 g/cc, and $\Delta t \sim 100$ ps = 10^{-10} s. So, $\Omega \sim 2 \times 10^{11}$ s^{-1}. Assuming an atomic number Z = 1 and average ion mass per proton mass of μ = 2.5 one finds from $\Omega = 9.58 \times 10^3 (Z/\mu)B$ in s^{-1} (NRL Plasma Formulary) a magnetic field strength of $B \sim 50$ MG which corresponds to a magnetic pressure of 100 Mbar. Since the stagnation pressure of a high-foot implosion is 100-200 Gbar, we expect the presence of magnetic fields to be unimportant in terms of stagnation properties.

Simulations showing various stages of the implosion for N140819 with magnetic field generation are shown in Figures 5 & 6. The net simulated fusion metrics for N140819 with (without) magnetic fields are: Y = 1.45e17 (1.46e17), DSR = 4.1% (4.1%), BT = 15.27 ns (15.28 ns), and T_{ion} = 6.6 keV (6.61 keV). As expected, no effect of the magnetic field is apparent in the fusion metrics, nor the morphology of the implosion as compared to the same implosion simulated with no magnetic field self-generation. The magnetic field strength is about 1/3 of the analytic estimate shown above. The structure of the self-generated magnetic field is interesting however and may have an effect on charged particles leaving the implosion.

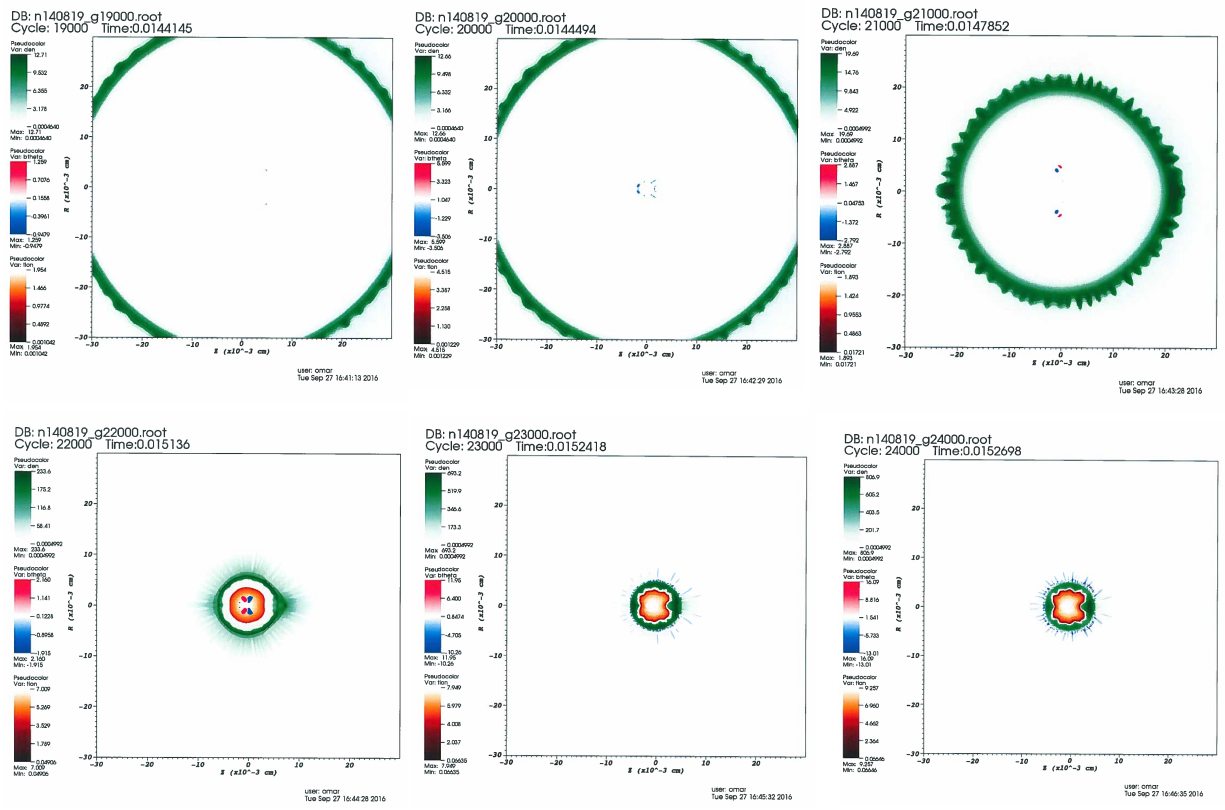

Figure 5: Shot N140819 - Density in the green color scale in g/cc, ion temperature in the orange color scale in keV, and the magnetic field in red-blue color scale in Mega-Gauss. The z-symmetry-axis is horizontal in these images. Time is shown in micro-seconds. As the shockwave in the DT (not visible here) impacts *r=0* with a slight asymmetry, some magnetic field is generated at the 1-2 MG level. Significantly more magnetic field, ~16 MG, is generated as the rebounding outward traveling shockwave exits the shell. The spike of shell material on the right hand side of the last two images is a result of a capsule defect feature included in the initial contour of the ablator inner and outer surface.

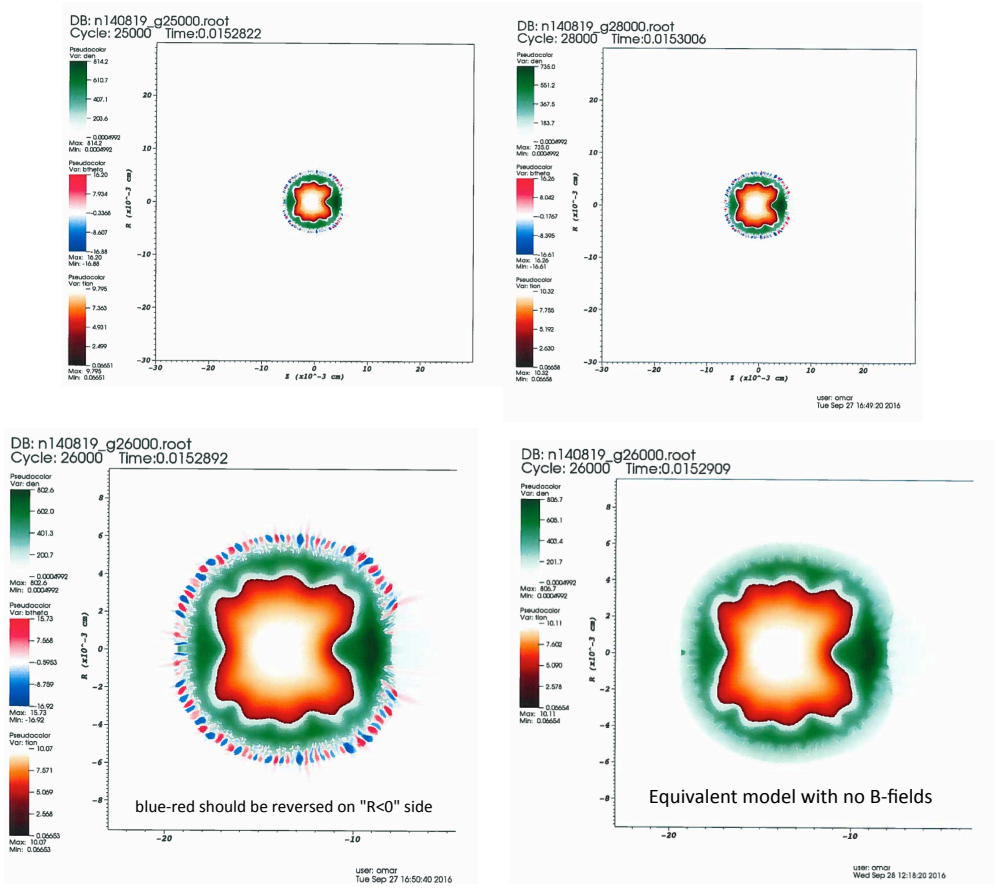

Figure 6: Shot N140819 - Density in the green color scale in g/cc, ion temperature in the orange color scale in keV, and the magnetic field in red-blue color scale in Mega-Gauss. The z-symmetry-axis is horizontal in these images. Time is shown in micro-seconds. (Upper) A couple more frames showing from time evolution in Fig. 5. (Lower left) A zoom-in image of the implosion around peak compression (bang-time = 15.28 ns). Magnetic field is concentrated around the perimeter of the shell with alternating B_θ that has a mode that corresponds to the Rayleigh-Taylor growth mode on the surface of the shell. Because the VISIT plotting software does not "understand" that magnetic field is a vector quantity, the polarity of the magnetic field in the lower half ($R<0$) of the frame is incorrectly colored with blue and red reversed. (Lower right) An identical simulation run with no self-generated magnetic fields shows identical morphology to the simulation with self-generated magnetic fields confirming that the presence of magnetic fields has no structural impact on the implosion.

Conclusions

In summary, ARES "capsule only" simulations demonstrate results of applying an ASC code to a suite of high-foot ICF implosion experiments. While a capability to apply an asymmetric FDS drive to the capsule-only model using add-on Python routines exists, it was not exercised here.

The ARES simulation results resemble the results from HYDRA simulations documented in A. Kritcher, et al., *Phys. Plasmas*, **23**, 052709 (2016). Namely, 1D simulation and data are in reasonable agreement for the lowest velocity experiments, but diverge from each other at higher velocities.